ChemComm

COMMUNICATION

View Article Online
View Journal | View Issue

Cite this: *Chem. Commun.*, 2025, **61**, 6639

Received 22nd February 2025,
Accepted 28th March 2025

DOI: 10.1039/d5cc00981b

rsc.li/chemcomm

Anhydrous salts for non-corrosive aluminium battery electrolytes†

Tomooki Hosaka *[a] and Patrik Johansson [ab]

Commercial aluminium triflate and aluminium bis(trifluoromethanesulfonyl)imide salts are hydrates, which renders water containing electrolytes that passivate electrodes through $Al(OH)_3$ formation. By acid–base reactions we produce anhydrous salts and the resulting anhydrous electrolytes demonstrate enhanced electrochemical activity, paving the way for aluminium battery development.

Rechargeable aluminium batteries (AlBs) have garnered significant attention in recent years due to the vast theoretical capacity of Al metal electrodes and the crustal abundance of Al.[1] While the negative electrode reactions of Al plating and stripping are fundamental to AlBs, they can only be achieved in a few electrolytes at room temperature,[2,3] most often chloroaluminate ionic liquids, such as $AlCl_3$ and 1-ethyl-3-methylimidazolium chloride (EMImCl) mixtures.[4,5] However, the highly corrosive nature of these electrolytes presents a significant barrier to study and develop electrode materials and make practical AlBs.[6] This has prompted extensive research efforts toward developing less corrosive electrolytes.[6–11]

A fundamental approach to address this challenge is to use non-corrosive or less-corrosive aluminium salts, such as aluminium triflate ($Al(OTf)_3$)[7,10–12] and aluminium bis(trifluoromethanesulfonyl)imide ($Al(TFSI)_3$).[6,8] However, for $Al(OTf)_3$, its hygroscopic nature and hydration have been reported to hinder the reversible Al plating/stripping.[13,14] Moreover, dehydration of $Al(OTf)_3$ is challenging due to decomposition upon heating to the temperature needed.[13] Indeed, hydration is a common issue for aluminium salts, in particular for those with monovalent bulky anions, due to strong Al^{3+}–water interactions and cation–anion size mismatch.[13,15] As for $Al(TFSI)_3$, that recently has become commercially available, the same issues can be expected. In this study, we investigate commercial, hydrated, $Al(OTf)_3$ and $Al(TFSI)_3$ and the impact of the water on the electrochemical reactions, and how anhydrous salt synthesis and subsequent use can improve performance.

Based on a previous report on the synthesis of $Al(TFSI)_3$,[16] anhydrous $Al(TFSI)_3$ and $Al(OTf)_3$ were synthesized in a water-free atmosphere through acid–base reactions between $Al(C_2H_5)_3$ and the corresponding acids (ESI†). Commercial $Al(OTf)_3$ from Sigma Aldrich and Thermo Fisher Scientific, and $Al(TFSI)_3$ from Boron Molecular were used as received. We start by examining and comparing the hydration of the different salts, followed by creation and characterisation of various non-aqueous electrolytes, and finally we demonstrate the resulting electrochemical differences and elucidate the mechanisms behind.

The commercial $Al(TFSI)_3$ and $Al(OTf)_3$ salts exhibit characteristic O–H stretching and H_2O bending peaks in their infrared spectra (Fig. 1a and b), clearly showing their hydrated state. In contrast, the salts synthesized have no such signatures and hence successful preparation of anhydrous compounds is verified. The water content was further quantified by Karl Fischer titration. Commercial $Al(OTf)_3$ and $Al(TFSI)_3$ contain *ca.* 3 and 5 moles of water per mole of salt, respectively, while the synthesized salts only 0.02–0.03 moles (Table S1, ESI†), resulting in 120–140 ppm water in 0.3 mol kg^{-1} (m) electrolytes (Table S2, ESI†). Reducing the water content in the salts even further is quite challenging due to their hygroscopic nature, making them to vividly absorb water from precursors and synthesis solvent(s), and perhaps also experimental equipment. Thus, reducing the water content in the electrolyte, which will be discussed later, is more practical.

To further verify successful and pure salt synthesis, the S/Al ratio was investigated using inductively coupled plasma atomic emission spectroscopy (ICP-AES). The synthesized $Al(OTf)_3$ and the commercial one from Aldrich showed S/Al ratios of 3.15 and 3.06, respectively, thus close to the theoretical 3.0 (Table S1, ESI†). In contrast, synthesized $Al(TFSI)_3$ and the one from Boron molecular showed some larger deviations from the theoretical 6.0 (Table S1, ESI†). Synthesized $Al(TFSI)_3$ (6.4) might have residual HTFSI or decomposition products of

[a] *Department of Physics, Chalmers University of Technology, 41296 Göteborg, Sweden. E-mail: hosaka@rs.tus.ac.jp*
[b] *ALISTORE-European Research Institute, CNRS FR 3104, Hub de l'Energie, Rue Baudelocque, 80039 Amiens, France*

† Electronic supplementary information (ESI) available. See DOI: https://doi.org/10.1039/d5cc00981b

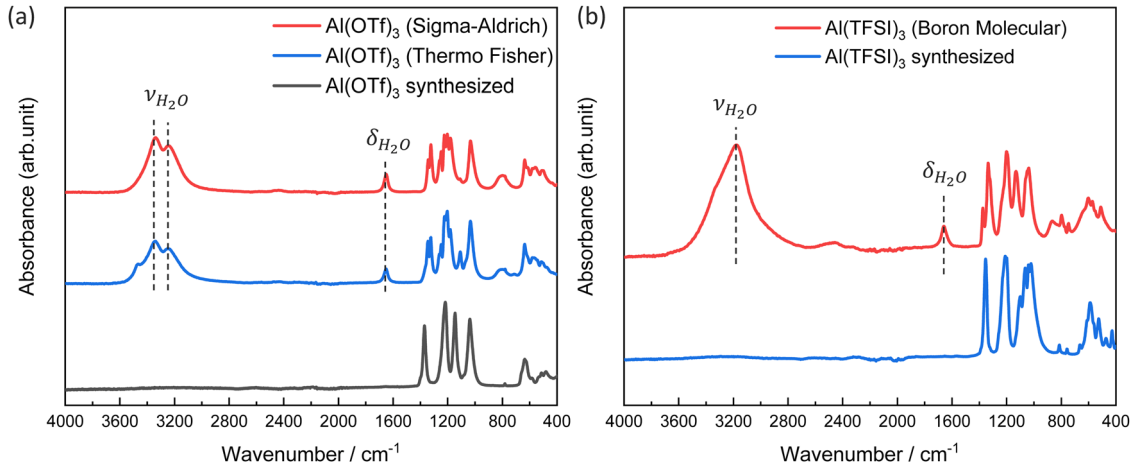

Fig. 1 ATR-FTIR spectra of commercial and synthesized (a) $Al(OTf)_3$ and (b) $Al(TFSI)_3$ salts.

HTFSI included, while the commercial salt (5.7) might have contamination by other anions, such as Cl^-. Thermal gravimetric analysis shows that the commercial $Al(TFSI)_3$ salts undergo an 80% weight loss at 150 °C (Fig. S1, ESI†), which we attribute to simultaneous decomposition and dehydration. Additionally, the temperature closely matches the decomposition temperature of the synthesized salt. Thus, as hypothesized above, simple thermal treatment is not a viable path to dehydrate $Al(TFSI)_3$, in analogy to $Al(OTf)_3$.[13]

0.3 m electrolytes were made by using acetonitrile (AN) and 1-butylimidazole (BIm) as solvents.[6,8] The infrared spectra of commercial $Al(OTf)_3$ and $Al(TFSI)_3$ in AN show a broad peak in the 2600–3600 cm^{-1} O–H stretching range, suggesting presence of an extensive hydrogen bond network involving H_2O and AN (Fig. 2a).

Using the C≡N stretching band region (Fig. 2b) pure AN has in fact two features, the C≡N stretch at 2253 cm^{-1} and an additional band at 2293 cm^{-1} from a combination of C–C stretch and CH_3 deformation modes.[17] Using the synthesized $Al(OTf)_3$ there are minor peaks of cation uncoordinated "free" AN, but significant peaks with notable blue shifts, at 2312 and 2339 cm^{-1} (Fig. 2b, #1 and #2), indicating strong Al^{3+}–AN coordination as it is similar what was reported previously for $AlCl_3$ in AN and attributed to $[AlCl(AN)_5]^{2+}$ and $[Al(AN)_6]^{3+}$.[18] In contrast, the spectrum of commercial $Al(OTf)_3$ shows comparatively more "free" AN and less coordinated AN (Fig. 2b). Moreover, the latter exhibited two additional peaks at 2304 and 2272 cm^{-1} (Fig. 2b, #3 and #4). The blue shift of the C≡N stretch band (~20 cm^{-1}) is larger than that of AN hydrogen-bonded to H_2O (~5 cm^{-1}),[19] but very similar to that of AN coordinated by Li^+ (~20 cm^{-1}).[20,21] Thus, it can be attributed to moderately strong interaction of AN with Al^{3+}, most probably in the second cation solvation shell. Similar results were observed for the $Al(TFSI)_3$ in AN electrolytes (Fig. S2, ESI†), demonstrating that Al^{3+} preferentially coordinates with H_2O over AN.

Similar to the AN electrolytes, the BIm electrolytes display clear signatures of direct Al^{3+}–BIm coordination,[22] but for the water containing electrolytes there is again broader peaks (Fig. S3, ESI†) indicating again that Al^{3+} preferentially

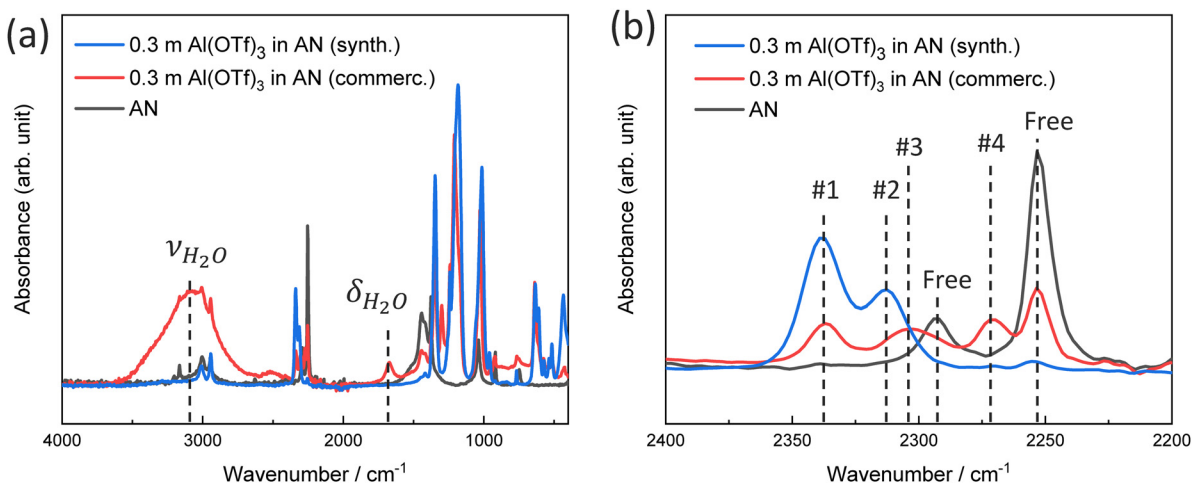

Fig. 2 ATR-FTIR spectra of 0.3 m commercial and synthesized (a) $Al(OTf)_3$ in AN and (b) enlarged figures in the range of 2400–2200 cm^{-1}.

coordinates with H_2O and Bim is relegated to the second or outer cation solvation shells. For all the electrolytes, the strong and preferential coordination between Al^{3+} and H_2O effectively hinders common attempts to eliminate the water – and will most likely also affect the electrochemical performance.

Turning to the electrochemistry, the open-circuit potential (OCP) using Al electrodes depends primarily on the solvent used than the salt employed (Table S3, ESI†). The AN electrolytes resulted in an OCP of *ca.* −1.1 V *vs.* Ag^+/Ag (−0.1 V *vs.* SHE), while the BIm electrolytes exhibited a more negative OCP of *ca.* −1.8 V *vs.* Ag^+/Ag (−0.8 V *vs.* SHE) The electrolyte of synthesized $Al(TFSI)_3$ in BIm showed the most negative OCP at −2.2 V *vs.* Ag^+/Ag (−1.2 V *vs.* SHE). These variations from the standard aqueous Al^{3+}/Al electrode potential (−1.66 V *vs.* SHE) stem from differences in solvation energy and ion pair formation, similar to what has been observed for $AlCl_3$-[EMIm]Cl electrolytes: −0.7 V *vs.* SHE for $AlCl_3$-[EMIm]Cl (2 : 1).[23]

In contrast, the cyclic voltammetry (CV) reveals clear differences between the commercial and synthesized salt based electrolytes; negligible activity for the former AN electrolyte and a reversible redox peak near 0 V *vs.* Al^{3+}/Al, indicating Al plating/stripping, for the corresponding latter electrolyte (Fig. 3a).

Somewhat similarly, the CV using a glassy carbon (GC) electrode shows the commercial $Al(OTf)_3$ based AN electrolyte to produce only a reduction peak, but no oxidation peak, and furthermore the current density decreased significantly below −0.8 V *vs.* Al^{3+}/Al, a clear signature of electrode passivation (Fig. 3b). In contrast, the corresponding synthesized salt based electrolyte enabled a quasi-reversible redox behaviour (Fig. 3b), although with a larger reduction overpotential than when using the Al electrode. While both were very low, the latter achieved a Coulombic efficiency of ∼40%, which is markedly higher than the ∼10% of the former (Fig. S4, ESI†). Qualitatively the commercial and synthesized $Al(TFSI)_3$ in AN electrolytes show similar trends, but the synthesized $Al(TFSI)_3$ electrolyte exhibits a lower current density than the $Al(OTf)_3$ counterpart. This can be due to the passivation effect by reductive anion decomposition or the salt impurities (Fig. S5, ESI†).

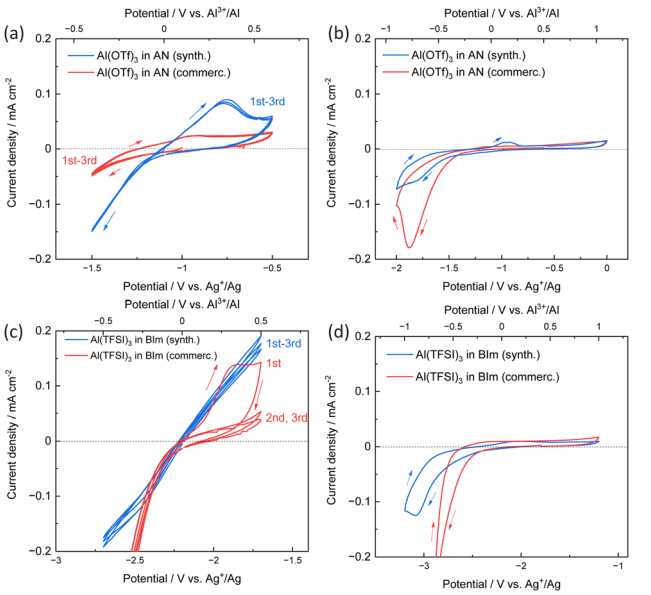

Fig. 3 CV of (a) Al and (b) GC working electrodes *vs.* 0.3 m $Al(OTf)_3$ in AN, and (c) Al and (d) GC working electrodes *vs.* 0.3 m $Al(TFSI)_3$ in BIm electrolytes.

Moving to the BIm electrolytes, the one based on synthesized $Al(TFSI)_3$ demonstrated a highly reversible behaviour when using an Al electrode between −0.5 and 0.5 V *vs.* Al^{3+}/Al (Fig. 3c). Using GC electrodes, the synthesized $Al(TFSI)_3$ in BIm electrolyte showed passivation near −0.8 V *vs.* Al^{3+}/Al (Fig. 3d), yielding *ca.* 50% lower Coulombic efficiencies (∼20%) than the AN electrolyte (Fig. S6, ESI†). While the current density is lower than that reported for the $[Al(BIm)_6][TFSI]_3$ electrolyte,[6] likely due to the lower operating temperature, the Coulombic efficiencies closely match, further supporting the passivation hypothesis. The commercial $Al(TFSI)_3$ in BIm electrolyte showed more than ten times higher reduction current using both Al and GC electrodes (Fig. S7, ESI†). Overall, side reactions, including water reduction, are promoted by the lower operating potential of the BIm electrolytes.

The above points to distinctly different degradation mechanisms at play for the different electrolytes. The water containing BIm electrolytes show electrochemical water reduction, whereas the corresponding AN electrolytes do not, suggesting passivation through chemical reactions between the aluminium metal electrode and electrolyte water – but both result in electrode passivation. To further investigate these passivation mechanisms, we conducted STEM and EELS analyses of an electrode subject to constant-potential electrodeposition using an $Al(TFSI)_3$ in BIm electrolyte. Cross-sectional STEM imaging revealed a ∼500 nm thick deposit containing both aluminium and oxygen throughout (Fig. 4a) and EELS confirmed the deposit to be Al_2O_3 (Fig. 4b).[24] For this, we have identified two possible formation pathways: (1) electrochemical water reduction generating hydroxide ions, followed by $Al(OH)_3$ precipitation with Al^{3+}, and (2) initial electrochemical metallic Al deposition followed by chemical reaction with water to form $Al(OH)_3$. Indeed, during the STEM sample preparation and analysis, the $Al(OH)_3$ precipitate likely dehydrated to form the observed Al_2O_3. Based on combining the CV and the STEM results, the first pathway appears to be the dominant mechanism when using the $Al(TFSI)_3$ in BIm electrolyte, whereas the second pathway likely dominates when using the AN electrolyte.

Finally, to further reduce the water content, we employed either an $Al(C_2H_5)_3$ water scavenger or a 3A molecular sieves treatment for the synthesized $Al(OTf)_3$ in AN (∼120 ppm water). Adding 0.01 m of $Al(C_2H_5)_3$ reduced the water content to ∼65 ppm, while the molecular sieve treatment achieved a significantly lower level of ∼20 ppm (Table S2, ESI†). However, the molecular sieves induced partial K^+/Na^+ and Al^{3+} ion exchange, as confirmed by the increased "free" AN peak in the FTIR spectra (Fig. S8, ESI†), suggesting a lower Al^{3+} concentration. The CV using an Al electrode shows these dry

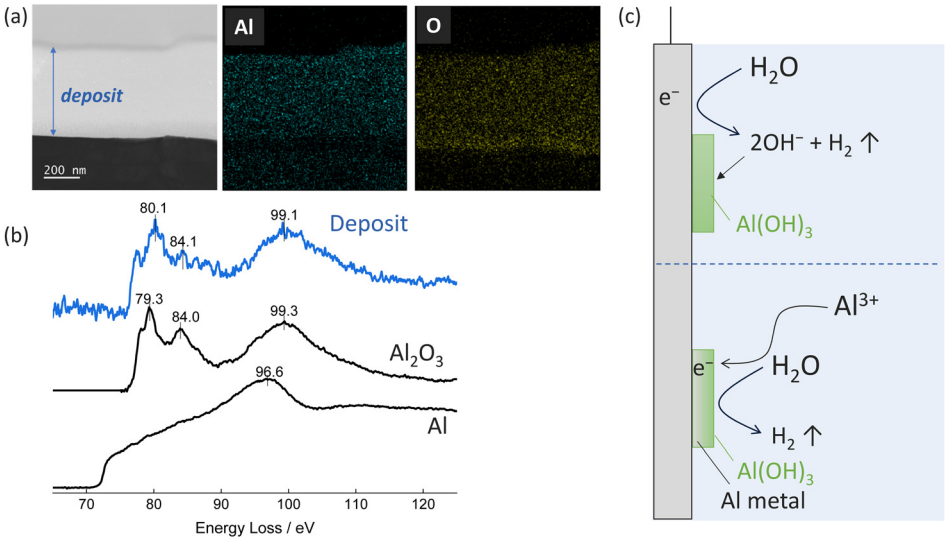

Fig. 4 (a) Cross-sectional STEM image and EDS mappings of a Pt electrode after constant potential electrodeposition. (b) Al-$L_{2,3}$ EELS spectra of the deposit. The Al_2O_3 and Al spectra were obtained from ref. 24. (c) Schematic illustration of possible reaction pathways to form $Al(OH)_3$ passivation layer.

electrolytes to demonstrate significantly higher current densities than the untreated electrolyte (Fig. S9, ESI†). Moreover, the $Al(C_2H_5)_3$ added electrolyte exhibited faster current decay than the molecular sieve-treated one, revealing a significant impact of the trace water on the passivation. In addition, the CV using the GC electrode shows much lower overpotential and a sharper peak at *ca.* 0 V *vs.* Al^{3+}/Al with higher Coulombic efficiency (~50%) in the molecular sieve treated electrolyte (Fig. S10, ESI†) than for the untreated electrolyte. Nevertheless, the current density was two orders of magnitude smaller than that in $AlCl_3$-[EMIm]Cl (2 : 1),[25] indicating a slow reaction rate.

In conclusion, while commercial $Al(OTf)_3$ and $Al(TFSI)_3$ salts only exist as hydrates, anhydrous salts, indeed possible to synthesize, are a prerequisite to avoid electrode passivation and maintain electrochemical activity. Yet, while we can demonstrate partially reversible electrochemistry on both Al and GC electrodes, the current density and Coulombic efficiency must be improved for any practical AlB application by electrolyte design, including the anion and solvent selection.

T. H. thanks Ms Mizuki Kawabe for her experimental assistance, and Prof. Shinichi Komaba, Dr Toshihiko Mandai, Dr Patricia Huijbers, Dr Zaher Slim, and Dr Ezio Zanghellini for fruitful discussions. This study was partially funded by JSPS KAKENHI (JP22K14772) and by the Swedish Research Council (grant #2021-00613). T. H. acknowledge JSPS Overseas Research Fellowships for financial support.

Data availability

Data for this article, including FTIR spectra, are available at Open Science Framework at DOI: **https://doi.org/10.17605/OSF.IO/XVBFJ**.

Conflicts of interest

There are no conflicts to declare.

Notes and references

1 N. Lindahl and P. Johansson, *Energy Adv.*, 2023, **2**, 420–429.
2 Y. Zhao and T. J. VanderNoot, *Electrochim. Acta*, 1997, **42**, 3–13.
3 T. Tsuda, G. R. Stafford and C. L. Hussey, *J. Electrochem. Soc.*, 2017, **164**, H5007.
4 P. K. Lai and M. Skyllas-Kazacos, *J. Electroanal. Chem. Interfacial Electrochem.*, 1988, **248**, 431–440.
5 T. Jiang, M. J. Chollier Brym, G. Dubé, A. Lasia and G. M. Brisard, *Surf. Coat. Technol.*, 2006, **201**, 1–9.
6 T. Mandai and P. Johansson, *J. Phys. Chem. C*, 2016, **120**, 21285–21292.
7 T. Mandai and P. Johansson, *J. Mater. Chem. A*, 2015, **3**, 12230–12239.
8 M. Chiku, S. Matsumura, H. Takeda, E. Higuchi and H. Inoue, *J. Electrochem. Soc.*, 2017, **164**, A1841.
9 X. Wen, J. Zhang, H. Luo, J. Shi, C. Tsay, H. Jiang, Y.-H. Lin, M. A. Schroeder, K. Xu and J. Guo, *J. Phys. Chem. Lett.*, 2021, **12**, 5903–5908.
10 F. Rahide, J. K. Flowers, J. Hao, H. S. Stein, H. Ehrenberg and S. Dsoke, *J. Electrochem. Soc.*, 2023, **170**, 120534.
11 Z. Slim and E. Menke, *Batter. Supercaps*, 2023, **6**(9), e202300164.
12 W. Peters, H. Thu Duong, S. Lee and J.-F. Drillet, *Phys. Chem. Chem. Phys.*, 2021, **23**, 21923–21933.
13 G. R. Pastel, Y. Chen, T. P. Pollard, M. A. Schroeder, M. E. Bowden, A. Zheng, N. T. Hahn, L. Ma, V. Murugesan, J. Ho, M. Garaga, O. Borodin, K. Mueller, S. Greenbaum and K. Xu, *Energy Environ. Sci.*, 2022, **15**, 2460–2469.
14 M. Talari, A. Sarapulova, E. Zemlyanushin, N. Sabi, A. Hofmann, V. Trouillet and S. Dsoke, *Batter. Supercaps*, 2025, **8**, e202400317.
15 V. M. Goldschmidt, *Trans. Faraday Soc.*, 1929, **25**, 253–283.
16 P. Eiden, Q. Liu, S. Zein El Abedin, F. Endres and I. Krossing, *Chem. – Eur. J.*, 2009, **15**, 3426–3434.
17 W. R. Fawcett and G. Liu, *J. Phys. Chem.*, 1992, **96**, 4231–4236.
18 J.-S. Seo, K.-W. Kim and H.-G. Cho, *Spectrochim. Acta. A. Mol. Biomol. Spectrosc.*, 2003, **59**, 477–486.
19 J. E. Bertie and Z. Lan, *J. Phys. Chem. B*, 1997, **101**, 4111–4119.
20 J. Barthel, R. Buchner and E. Wismeth, *J. Solut. Chem*, 2000, **29**, 937–954.
21 X. Xuan, H. Zhang, J. Wang and H. Wang, *J. Phys. Chem. A*, 2004, **108**, 7513–7521.
22 J. Reedijk, *Inorg. Chim. Acta*, 1969, **3**, 517–522.
23 S. Wang, K. V. Kravchyk, A. N. Filippin, U. Müller, A. N. Tiwari, S. Buecheler, M. I. Bodnarchuk and M. V. Kovalenko, *Adv. Sci.*, 2018, **5**, 1700712.
24 D. Bouchet and C. Colliex, *Ultramicroscopy*, 2003, **96**(2), 139–152.
25 M. Zhang, J. S. Watson, R. M. Counce, P. C. Trulove and T. A. Zawodzinski, *J. Electrochem. Soc.*, 2014, **161**, D163.

